Histochem Cell Biol (2013) 140:549–566
DOI 10.1007/s00418-013-1093-x

ORIGINAL PAPER

GABAergic signaling in the pulmonary neuroepithelial body microenvironment: functional imaging in GAD67-GFP mice

Kathy Schnorbusch · Robrecht Lembrechts · Isabel Pintelon · Jean-Pierre Timmermans · Inge Brouns · Dirk Adriaensen

Accepted: 26 March 2013 / Published online: 9 April 2013

Abstract Gamma-aminobutyric acid (GABA) is the main inhibitory neurotransmitter in the central nervous system (CNS) of vertebrates, but has also been reported in multiple cell types outside the CNS. A GABAergic system has been proposed in neuroepithelial bodies (NEBs) in monkey lungs. Pulmonary NEBs are known as complex intraepithelial sensory airway receptors and are part of the NEB microenvironment. Aim of the present study was to unravel a GABAergic signaling system in the NEB microenvironment in mouse lungs, enabling the use of genetically modified animals for future functional studies. Immunostaining of mouse lungs revealed that glutamic acid decarboxylase 65/67 (GAD65/67), a rate-limiting enzyme in the biosynthesis of GABA, and the vesicular GABA transporter (VGAT) were exclusively expressed in NEB cells. In GAD67-green fluorescent protein (GFP) knock-in mice, all pulmonary NEBs appeared to express GFP. For confocal live cell imaging, ex vivo vibratome lung slices of GAD67-GFP mice can be directly loaded with fluorescent functional probes, e.g. a red-fluorescent calcium dye, without the necessity of time-consuming prior live visualization of NEBs. RT-PCR of the NEB microenvironment obtained by laser microdissection revealed the presence of both $GABA_A$ and $GABA_B$ (R1 and R2) receptors, which was confirmed by immunostaining. In conclusion, the present study not only revealed the presence of a GABAergic signaling pathway, but also the very selective expression of GFP in pulmonary NEBs in a GAD67-GFP mouse model. Different proof of concept experiments have clearly shown that adoption of the GAD67-GFP mouse model will certainly boost future functional imaging and gene expression analysis of the mouse NEB microenvironment.

Keywords NEB microenvironment · Mouse lungs · GABA · GABA receptors · GAD67-GFP mice · Confocal live cell imaging · Immunohistochemistry · Laser microdissection

K. Schnorbusch · R. Lembrechts · I. Pintelon · J.-P. Timmermans · I. Brouns · D. Adriaensen (✉)
Laboratory of Cell Biology and Histology, Department of Veterinary Sciences, University of Antwerp, Groenenborgerlaan 171, 2020 Antwerp, Belgium
e-mail: Dirk.Adriaensen@ua.ac.be

Introduction

Gamma-aminobutyric acid (GABA) is an amino acid and the main inhibitory neurotransmitter in the central nervous system (CNS), acting via specific receptors. The GABA synthesis is controlled by two molecular forms of the rate-limiting enzyme glutamic acid decarboxylase (GAD), i.e. GAD65 and GAD67, both of which generate GABA. GAD65 and GAD67 are products of two separate genes, GAD2 and GAD1, respectively (Bu et al. 1992), and exhibit different subcellular localizations, functions, regulatory properties and co-factor interactions (Kaufman et al. 1991). GABA can be accumulated into synaptic vesicles by the vesicular GABA transporter [VGAT; (McIntire et al. 1997)], an apparently fundamental aspect of GABAergic transmission (Saito et al. 2010), and functions can be triggered both by binding to the ionotropic $GABA_A$ and $GABA_C$ receptors that are ligand-gated chloride channels, and to the metabotropic $GABA_B$ receptors that are obligatory heterodimers comprising two distinct subunits, $GABA_BR1$ and $GABA_BR2$ (Bormann 2000). Over the years, it has become clear that GABA has roles beyond synaptic neurotransmission in the CNS and is known to

control secretion in peripheral organs, to act as a signaling molecule in both embryonic developing and adult regenerating tissues, and is believed to be involved in the control of stem/cancer cell proliferation (Young and Bordey 2009). Green fluorescent protein (GFP)-based visualization has been applied to study GABAergic neurons in the CNS using transgenic mice harboring GFP expression driven by the GAD67 promoter (Oliva et al. 2000; Zhao et al. 2010). A similar mouse strain was reported to show the presence of fluorescent cell groups, reminiscent of neuroepithelial bodies (NEBs) in the lungs (Yabumoto et al. 2008).

NEBs (Lauweryns et al. 1972) are clusters of pulmonary neuroendocrine cells (PNECs) that are widely distributed within the intrapulmonary airway epithelium of man, mammals and all other air-breathing vertebrate groups (Sorokin and Hoyt 1989; Adriaensen et al. 2003; Brouns et al. 2012). NEBs show an extensive and selective innervation (Adriaensen et al. 2006; Brouns et al. 2009) and store various bioactive substances, e.g. monoamine, peptide, and purine transmitters, in cytoplasmic dense-cored secretory granules (Scheuermann 1987). Upon appropriate stimulation these substances can be secreted and may interact with NEB-associated nerve terminals and surrounding cells, or may be taken up by nearby blood capillaries. Specialized Clara cells, the Clara-like cells (CLCs), reside exclusively around and over NEBs, and compose together with the innervation and PNECs, the so-called NEB microenvironment (De Proost et al 2008). Intriguingly, the exact role of NEBs in the healthy lung is still under debate. Based on mainly morphological data, several hypotheses have been suggested and are still actively studied (Linnoila 2006; Adriaensen et al. 2003; Cutz and Jackson 1999; Sorokin and Hoyt 1990). In general, NEBs are believed to exert diverse functions during pre-, neo- and postnatal life, which may be further modulated by their extensive innervation and the local environment (Adriaensen et al. 2003; Lauweryns and Van Lommel 1986). To date, comprehensive evidence implicates pulmonary NEBs in airway oxygen sensing, mainly in the perinatal period, in different species (Cutz and Jackson 1999; Cutz et al. 2003), including mice (Fu et al. 2000), but also in cell models (Kemp et al. 2003). Recently, considerable evidence has also been obtained for the involvement of the NEB microenvironment in airway mechanosensing (Pan et al. 2006; Lembrechts et al. 2011, 2012).

The past few years, we optimized a confocal live cell imaging (LCI) model based on murine lung vibratome slices, which allows identification and manipulation of NEBs while visualizing and recording changes in mitochondrial membrane potential using the red-fluorescent styryl pyridinium dye 4-(4-diethylaminostyryl)-*N*-methylpydridinium iodide [4-Di-2-ASP (Pintelon et al. 2005; De Proost et al. 2008)]. Simultaneously, real-time alterations in the intracellular calcium concentration ($[Ca^{2+}]_i$) in NEB cells and surrounding airway epithelial cells can be visualized using a green-fluorescent Ca^{2+}-indicator (De Proost et al. 2008). It was demonstrated that Ca^{2+}-mediated activation of NEB cells is followed by exocytosis of neurotransmitters, visualized by a delayed $[Ca^{2+}]_i$ rise in the neighboring CLCs, which appears to be driven by ATP secreted from NEBs (De Proost et al. 2009; Lembrechts et al. 2012).

The existence of a GABAergic system has been proposed for NEBs in monkey lungs (Fu and Spindel 2009), but little is known about the exact location and identity of GABA producing cells, GABA receptors and their relevance in the healthy NEB microenvironment. The present study intended to obtain detailed information on the potential GABAergic signaling system in mouse airway epithelium, enabling the future use of genetically modified GAD-GFP mouse models that would offer new possibilities for targeted physiological and gene expression studies.

Materials and methods

Animals

Lung tissue was obtained from wild-type (wt) C57-Bl6 mice (Janvier, Bio Services, Uden, The Netherlands) and B6.Cg-Tg(Gad1-EGFP)3Gfng/J mice (JAX 007673; The Jackson Laboratory, Charles River, l'Arbresle, France). The latter is a C57-Bl6 based GAD67-EGFP knock-in mouse strain, further on referred to as 'GAD67-GFP mice'. Numbers and ages of the animals are specified in the respective sections.

All animals were housed with their mothers in acrylic cages in an acclimatized room (12/12 h light/dark cycle; 22 ± 3 °C) and were provided with water and food ad libitum. National and European principles of laboratory animal care were followed and experiments were approved by the local animal ethics committee of the University of Antwerp. All mice were killed at the start of each of the further described experimental procedures by an overdose of sodium pentobarbital (Nembutal 200 mg/kg; CEVA Santé Animale, Brussels, Belgium) containing heparin (500 U/kg; Rhône Poulenc Rorer 256S68F12; Brussels, Belgium).

Immunohistochemical staining

Tissue processing

The pulmonary circulation of wt C57-Bl6 mice [embryonic day 18 (ED18 ($n = 3$)), postnatal day 21 (PD21 ($n = 3$))

and adult ($n = 3$)] and GAD67-GFP mice [ED18 ($n = 3$), PD21 ($n = 5$) and adult ($n = 3$)] was perfused with physiological solution and the lungs were intratracheally instilled with 4 % paraformaldehyde (0.1 M phosphate buffer; pH 7.4). Lungs, trachea, esophagus and heart were dissected en bloc, degassed and further immersion-fixed in the same fixative for 2 h. As a positive control, brains of GAD67-GFP mouse [PD21 ($n = 2$)] were removed after intracardial perfusion with physiological solution, followed by 4 % paraformaldehyde (0.1 M phosphate buffer; pH 7.4) and were further processed as described for lungs.

After rinsing in phosphate-buffered saline (PBS 0.01 M, pH 7.4), the tissue blocs were stored overnight in 20 % sucrose (in PBS, 4 °C) and subsequently mounted in Tissue Tek (Sakura Finetek Europe, Zoeterwoude, the Netherlands) on a cryostat chuck by freezing in a CO_2 chamber. Serial 25-µm-thick cryostat sections of the lung and brain blocks were thaw-mounted on poly-L-lysine-coated microscope slides, dried at 37 °C (2 h), and either processed for immunolabeling or stored at −80 °C in a closed container until further use.

Immunohistochemical labeling

All immunohistochemical procedures were carried out at room temperature in a humid incubation chamber. Characteristics and sources of the applied primary antisera are listed in Table 1, those of secondary and tertiary antisera in Table 2. The combinations of primary and secondary antisera used for multiple immunostaining are listed in Table 3. Single immunostaining was carried out as outlined in the first step of the multiple staining procedures. Unless otherwise indicated, all antisera were diluted in PBS containing 10 % non-immune serum of the host species of the secondary antibodies, 0.1 % bovine serum albumin, 0.05 % thimerosal, and 0.01 % NaN_3 (PBS*). Prior to incubation with the primary antisera, cryostat sections were incubated for 30 min with PBS* containing 1 % Triton X-100. To block endogenous mouse IgG, sections were preincubated with PBS* containing mouse-on-mouse blocker (M.O.M., Vector Labs, Burlingame, CA, USA). When biotin-conjugated secondary antibodies were used for signal amplification, sections were pretreated with an avidin/biotin blocking kit (Invitrogen SA, Merelbeke, Belgium). Cryostat sections were routinely incubated overnight with the primary antibodies, rinsed in PBS and incubated for 4 h with the appropriate secondary antibodies. After a final wash all sections were mounted in citifluor (Ted Pella 19470, Redding, CA, USA).

Multiple immunohistochemical staining using tyramide signal amplification (TSA)

To enhance sensitivity and to allow the straightforward combination of two antisera raised in rabbits, biotin-conjugated tyramide signal amplification (TSA kit NEL700; PerkinElmer Life Sciences, Zaventem, Belgium) was applied. Between subsequent steps, sections were rinsed in PBS containing 0.05 % Tween 20. Prior to the immunohistochemical procedures, endogenous peroxidase activity in cryostat sections of mouse lungs was blocked by H_2O_2 (3 % in 50 % methanol in PBS; 10 min). Following incubation with the first primary antiserum (see Tables 1 and 3), sections were consecutively incubated with the appropriate biotinylated secondary antibodies for 1 h (see Table 2), with ExtrAvidin-horseradish peroxidase (in PBS, 1 h), biotin-conjugated tyramide (diluted 1:100 in 'amplification solution', 10 min), and fluorochrome-conjugated streptavidin (diluted 1:6,000, 10 min) to visualize the reaction. For double immunohistochemical stainings, the latter was followed by application of a second primary antiserum, detected using a conventional secondary antibody. For the simultaneous detection of three antigens, the first primary antiserum was detected using TSA, while the

Table 1 List of primary antisera used for immunohistochemistry

Primary antisera			
Antigen	Host	Mc/Pc	Source
Calbindin D-28k (CB)	Rabbit	Pc	Swant CB-38, Bellinzona, Switzerland
Calcitonin gene-related peptide (CGRP)	Mouse	Mc	Sigma C7113, Bornem, Belgium
CGRP	Rabbit	Pc	Sigma C8198
Clara cell specific protein (CCSP)	Rabbit	Pc	DakoCytomation A0257, DK-2600, Glostrup, Denmark
Gamma-aminobutyric acid B receptor R1 ($GABA_BR1$)	Rabbit	Pc	Abcam ab131417, Cambridge, UK
Gamma-aminobutyric acid B receptor R2 ($GABA_BR2$)	Rabbit	Pc	Abcam ab52248, Cambridge, UK
Glutamate decarboxylase 65/67 (GAD65/67)	Rabbit	Pc	Chemicon AB1511, Temecula, CA, USA
$P2X_3$ receptor ($P2X_3$)	Rabbit	Pc	Chemicon AB5895
Synaptophysin (SYN)	Guinea pig	Pc	Synaptic Systems 101 004, Göttingen, Germany
Vesicular GABA transporter (VGAT)	Rabbit	Pc	Synaptic Systems 131 003

Table 2 List of secondary antisera and streptavidin complexes used for immunohistochemistry

Secondary antisera, streptavidin complexes	Source	Dilution
Biotinylated Fab fragments of goat anti-rabbit IgG (GAR-Fab-BIOT)	Rockland 811-1602, Gilbertsville, PA, USA	1:500
Cy™3-conjugated Fab fragments of goat anti-rabbit IgG (GAR-Fab-Cy3)	Jackson ImmunoResearch 111-167-003, West Grove, PA, USA	1:2,000
Cy™3-conjugated streptavidin (STR-Cy3)	Jackson ImmunoResearch 016-160-084	1:6,000
Cy™5-conjugated Fab fragments of goat anti-rabbit IgG (GAR-Fab-Cy5)	Jackson ImmunoResearch 111-177-003	1:500
DyLight™488-conjugated Fab fragments of goat anti-rabbit IgG (GAR-Fab-DyLight488)	Jackson ImmunoResearch 111-487-003	1:500
DyLight™488-conjugated donkey anti-mouse IgG (DAM-DyLight488)	Jackson ImmunoResearch 715-485-151	1:500
ExtrAvidin™ horseradish peroxidase	Sigma E2886	1:1,000
FITC-AffiniPure donkey anti-guinea pig IgG (H + L) (DAGp-FITC)	Jackson ImmunoResearch 706-095-148	1:100

second and third primary antisera, raised in different species, were detected by conventional double immunocytochemical staining.

Control experiments for the immunohistochemical procedures

Negative staining controls for all immunohistochemical procedures were performed by substitution of primary or secondary antisera with non-immune sera. Controls for the amplification-based multiple staining were performed by omission of the primary antiserum of the second and third incubations. To check for possible cross-reactivity after consecutive multiple staining, the results of single immunostaining for the different antisera were evaluated and compared with those from multiple labeling experiments.

Laser microdissection and reverse transcriptase (RT)-PCR

Lungs of GAD67-GFP mice (PD14, $n = 3$) were dissected, snap-frozen in liquid nitrogen and preserved at −80 °C. 25-µm-thick cryosections were thaw-mounted on PET Frameslides (Leica, Wetzlar, Germany). NEB microenvironment and control airway epithelium were excised and collected from the slides by laser microdissection (LMD; Leica LMD7000 system). A mouse hippocampus sample was snap-frozen and processed together with the LMD samples as a positive control.

Total RNA of the LMD and hippocampus samples was isolated using the RNeasy Plus Micro kit (Qiagen, Hilden, Germany). Concentration and integrity of the RNA samples was evaluated by an Experion automated electrophoresis system (Bio-Rad, Hercules, CA, USA) using the Experion HighSens analysis kit. cDNA was prepared using the SuperScriptIII First-Strand Synthesis SuperMix (Invitrogen, Life Technologies, Gent, Belgium) on a MJ Mini Cycler (Biorad). Taqman gene expression analysis was used for RT-PCR analysis in a multiwell-plate-based system (LightCycler 480; LC480; Roche Applied Science, Penzberg, Germany). All reactions were carried out in real-time using gene-specific probes. The primer and probe design was based on the general guidelines for RT-PCR primer design using the Lasergene (DNASTAR) software. A BLAST analysis was performed to confirm the specificity of the primers and the probes. All primers were designed to be intron-spanning and to obtain an amplicon length of 60–150 bp (Table 4). RT-PCR was performed using the LC480 Probes Master (Roche Applied Science) in LC480 white 96 Multiwell Plates (Roche Applied Science). All samples were run in triplicate and no-template controls (blanco) were included in all runs. The eukaryotic translation elongation factor-2 (eEF-2) was used as a reference gene (Kouadjo et al. 2007). Amplification products were separated on a 2 % agarose gel and visualized under UV illumination.

Live cell imaging (LCI)

Drugs, solutions and perfusion

A standard physiological solution was used throughout the various LCI experiments, containing (in mM): NaCl, 130; KCl, 5; $CaCl_2{\cdot}2H_2O$, 1.2; $MgSO_4{\cdot}7H_2O$, 1; D-glucose, 11; HEPES, 20; 290 mosmol; pH 7.4 adjusted with NaOH. The osmolarity of all solutions was maintained between 285 and 300 mosmol since our recent studies revealed activation of NEB cells by hypo-osmotic (230 mosmol) solutions (Lembrechts et al. 2012). Solutions containing a high extracellular potassium concentration ($[K^+]_o$) were prepared by equimolar substitution of KCl for NaCl. Chemicals and drugs were purchased from Sigma-Aldrich (Bornem, Belgium), unless indicated otherwise. All stimuli were applied to lung slices that were submerged in a tissue

Table 3 List of applied immunocytochemical double and triple staining procedures

Multiple stainings								
Conventional single staining								
Primary antisera antigen 1				Dilution				Visualization
CGRP				1:5,000				GAR-Fab-Cy3
$P2X_3$				1:1,000				GAR-Fab-Cy3
CB				1:1,000				GAR-Fab-Cy3
$GABA_BR1$				1:2,000				GAR-Fab-Cy3
$GABA_BR2$				1:200				GAR-Fab-Cy3
Conventional double staining								
Primary antisera antigen 1		Dilution	Visualization	Primary antisera antigen 2		Dilution		Visualization
VGAT		1:4,000	GAR-Fab-Cy3	Synaptophysin		1:4,000		DAGp-FITC
VGAT		1:4,000	GAR-Fab-Cy3	CGRP		1:2,000		DAM-Dylight488
Double staining with one tyramide signal amplification (TSA)								
Primary antisera antigen 1 (TSA)		Dilution	Visualization	Primary antisera antigen 2 (conv.)		Dilution		Visualization
GAD65/67		1:6,000	STR-Cy3	CGRP		1:5,000		GAR-Fab-Dylight488
GAD65/67		1:6,000	STR-Cy3	CGRP		1:5,000		GAR-Fab-Cy5
Triple labeling using TSA and conventional staining								
Primary antisera antigen 1 (TSA)	Dilution	Visualization	Primary antisera antigen 2 (Conv.)	Dilution	Visualization	Primary antisera antigen 3 (Conv.)	Dilution	Visualization
GAD65/67	1:6,000	STR-Cy3	CGRP	1:2,000	DAM-Dylight488	CB	1:1,000	GAR-Fab-Cy5
GAD65/67	1:6,000	STR-Cy3	CGRP	1:2,000	DAM-Dylight488	CCSP	1:200	GAR-Fab-Cy5

Table 4 List of primers and probes used for RT-PCR

Gene	Primer/probe	Sequence
$GABA_A\beta3$	$GABA_A\beta3$ FP	CTCCCACAGTTCTCCATTGTAG
	$GABA_A\beta3$ RP	GGATTGAGGGCATATACGTCTG
	$GABA_A\beta3$ probe	FAM-TTGTCTTCGCCACAGGTGCC TATC-BBQ
$GABA_BR1$	$GABA_BR1$ FP	CACCGAACCATTGAGACTTTTG
	$GABA_BR1$RP	GCAGCCCTTTGTAACCATAGA
	$GABA_BR1$ probe	FAM-TGATGTCTCCATTCTGCCCC AGC-BBQ
$GABA_BR2$	$GABA_BR2$ FP	CCAGGACTTCAACTACACAGAC
	$GABA_BR2$ RP	TTCCCATTCTTTCCCCGTTC
	$GABA_BR2$ probe	FAM-CACAACTTGACCCGTGACT CCGA-BBQ

FP forward primer, *RP* reverse primer

bath (2 ml) mounted on the microscope stage, perfused by a gravity-fed system (flow rate of >5 ml/min) with triggered valves that allowed the fast and reproducible exchange of solutions.

Preparation of lung slices

After killing the animals as described above, vibratome slices of GAD67-GFP mice (PD14; $n = 19$) were cut from separate lung lobes as previously published (De Proost et al. 2008; Pintelon et al. 2005). In short, lung tissue was stabilized by instilling a 2 % agarose solution (low-melt agarose; A4018, Sigma) via a tracheal cannula. After inflation, lungs were dissected and transferred to ice-cold physiological solution to enable complete gelling of the agarose. Lung slices (100–150 μM thick) were cut using a vibratome (HM650V; Microm International, Walldorf, Germany) with cooled tissue bath (4 °C). All lung slices were incubated in Dulbecco's modified Eagle's medium/F12 (DMEM-F-12; Gibco, Invitrogen, Merelbeke, Belgium) at 37 °C, and used within 12 h of killing the animal.

Receptor binding to a fluorescent agonist

Muscimol is a powerful agonist of the $GABA_A$ receptor and has been widely used to reversibly inactivate localized groups of neurons (Majchrzak and Di 2000). Using red-fluorescent BODIPY TMR-X muscimol (M23400, Invitrogen), the presence of functional $GABA_A$ receptors can be detected at the plasma membrane (Borodinsky and Spitzer 2007). Vibratome lung slices were incubated for 1 h at room temperature in standard physiological solution with 10 μM BODIPY TMR-X muscimol (dissolved in DMSO, with an end-concentration of 0.05 %). The slices were subsequently washed (10 min) in standard physiological solution.

Fig. 1 **a–i** Double immunolabeling for GAD65/67 (*red* Cy3 fluorescence) and CGRP (*green* Dylight488 fluorescence), a marker for NEB cells, in cryosections of prenatal (ED18; **a–c**), 3-week-old (PD21; **d–f**) and adult (**g–i**) mouse lungs. **a**, **d**, **g** *Red* channels showing GAD65/67 expressing epithelial cell groups. **b**, **e**, **h** CGRP-immunoreactive (ir) NEBs and associated nerve terminals. **c**, **f**, **i** Combination of the *red* and *green* channel revealing that all NEBs express GAD65/67. **j–m** Triple immunolabeling for GAD65/67 (*red* Cy3 fluorescence), CGRP (*green* Dylight488 fluorescence) and calbindin D-28k (CB; artificial *blue* color for Cy5 emission in far red), as a marker for a subpopulation of the myelinated vagal sensory innervation of mouse pulmonary NEBs. **j** GAD65/67-ir intraepithelial cell group. **k** CGRP-ir NEB cells. **l** CB expression in intraepithelial nerve terminals. **m** Combined *red*, *green* and *blue* channels showing a GAD65/67 (*arrowheads*) and CGRP (*open arrowheads*) expressing NEB, which is innervated by CB-ir vagal sensory nerve terminals that protrude between (*arrows*) and surround the NEB cells. Note that the CB-ir nerve fiber population lacks GAD65/67. **n–q** Triple immunolabeling for GAD65/67 (*red* Cy3 fluorescence), CGRP (*green* Dylight488 fluorescence) and Clara cell secretory protein (CCSP; artificial *blue* color for Cy5 emission in far red), a marker for Clara and Clara-like cells in mouse airways. **n** GAD65/67-ir intraepithelial cell group. **o** CGRP-ir NEB cells. **p** CCSP expression in airway epithelial cells. Note the absence of CCSP from NEB cells. Clara-like cells are marked (*asterisks*). **q** Combination of the three channels revealing that in the NEB microenvironment GAD65/67 is expressed by NEB cells only *L* lumen of an airway

Specific staining of NEBs in live lung slices and mitochondrial membrane potential indicator loading procedure

Loading was performed as previously published (Pintelon et al. 2005). In short, lung slices were incubated for 4 min with 4 μM 4-Di-2-ASP (D289, Invitrogen) in DMEM-F-12 at 37 °C, rinsed and subsequently kept in DMEM-F-12 until further manipulation and LCI.

Ca^{2+} indicator loading procedure

Lung slices were incubated in standard physiological solution with the red-fluorescent Ca^{2+} indicator dye GFP-certified FluoForte Reagent (FluoForte; 10 μM; ENZ-52016-5C50, Enzo Life Sciences, Zandhoven, Belgium), 100 μM sulfobromophthalein, 0.1 % DMSO and 0.02 % Pluronic F-127, for 1 h at room temperature (RT). The slices were subsequently washed (10 min, RT) in standard physiological solution with 100 μM sulfobromophthalein.

Microscopic data acquisition

An epifluorescence microscope (Zeiss Axiophot; Carl Zeiss, Jena, Germany) equipped with filters for the visualization of green- (Zeiss 17; BP 485-520/FT 510/BP 515-565) and red-fluorescent labels (Zeiss 00; BP530-585/FT 600/LP 615) was used to quickly evaluate the immunostaining results.

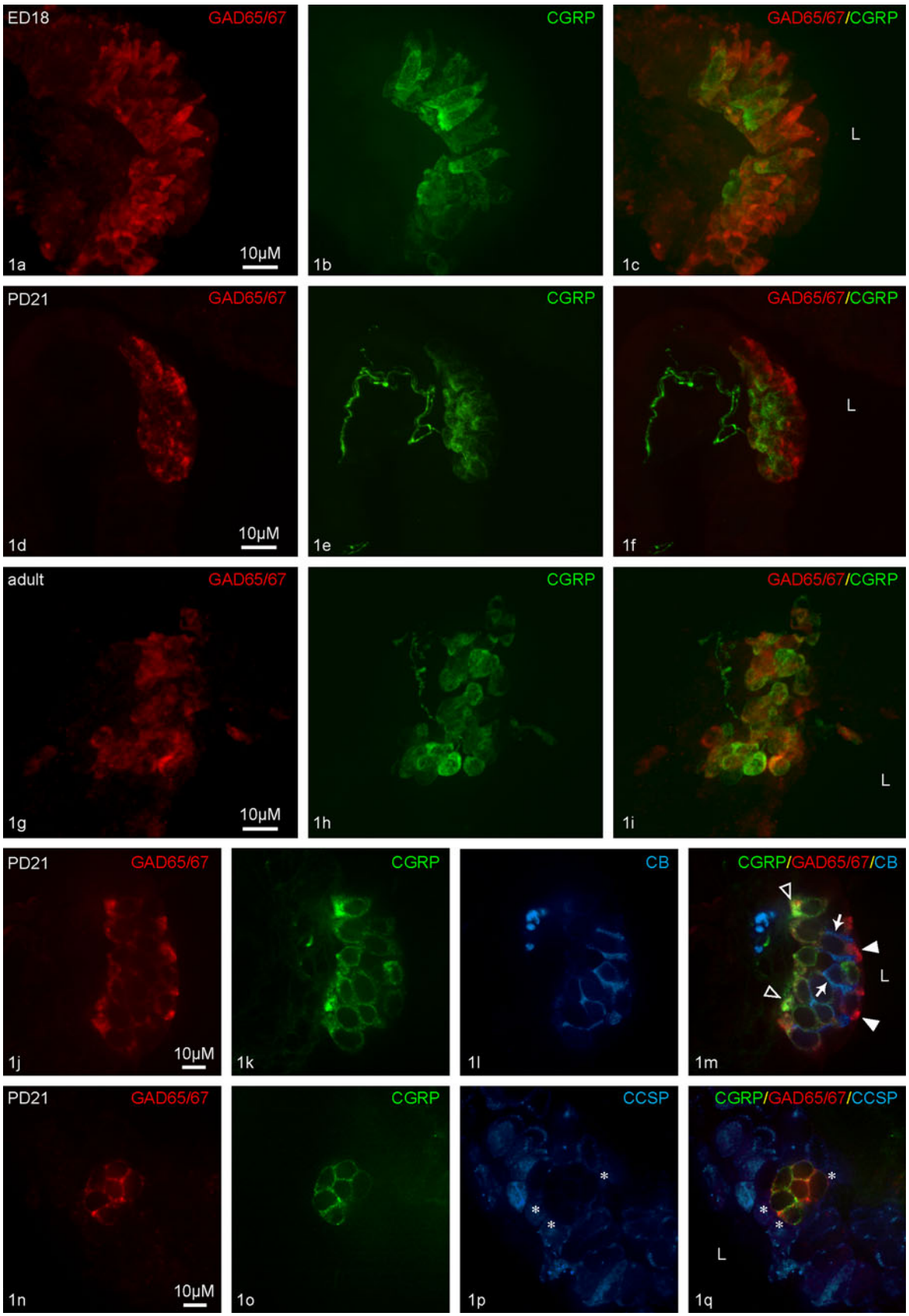
ED18
GAD65/67
10μM
1a
CGRP
1b
GAD65/67/CGRP
L
1c
PD21
GAD65/67
10μM
1d
CGRP
1e
GAD65/67/CGRP
L
1f
adult
GAD65/67
10μM
1g
CGRP
1h
GAD65/67/CGRP
L
1i
PD21
GAD65/67
10μM
1j
CGRP
1k
CB
1l
CGRP/GAD65/67/CB
L
1m
PD21
GAD65/67
10μM
1n
CGRP
1o
CCSP
1p
CGRP/GAD65/67/CCSP
L
1q

All high-resolution images and LCI results were obtained using a Nikon Eclipse Ti-E inverted microscope attached to a microlens-enhanced dual spinning disk confocal system (Ultra*VIEW* VoX; PerkinElmer, Zaventem, Belgium) equipped with 488, 561 and 640 nm diode lasers for excitation of green, red and far-red fluorophores, respectively. For physiological LCI experiments, lung slices were transferred to the perfusion chamber on the microscope stage and were restrained with a golden ring spanned with a sheet of nylon mesh. To avoid phototoxicity and photobleaching, laser illumination was kept to a minimum. Time-lapse images of changes in both 4-Di-2-ASP and FluoForte fluorescence were captured (2 images/s) using the 561 nm laser line for excitation while the emitted fluorescence was selected by a red emission filter (dichroic mirror 488/561/640; band pass 580–650). High-resolution images and LCI results of GFP-fluorescent NEBs were obtained using the 488 nm laser line for excitation while the emitted fluorescence was selected by a green emission filter (dichroic mirror 488/661/640; band pass 500–555).

Data analysis

Images and time-lapse recordings were acquired and processed using Volocity 6.0.1 software (Improvision, PerkinElmer). For analysis of the time-lapse recordings, individual images were studied as grey value datasets. Regions of interest (ROIs) were drawn manually around identified cells of interest. For every ROI, the fluorescence intensity, expressed as arbitrary units (AU), was plotted against time. To facilitate interpretation of the results, grey levels were adjusted for the basal level of fluorescence that was present at the start of imaging. 4-Di-ASP and FluoForte are non-ratiometric dyes, and all changes in fluorescence values should be seen as qualitative changes in mitochondrial potential or $[Ca^{2+}]_i$. The graphs shown are representative for multiple experiments performed under the respective conditions.

Fig. 3 **a** Image of a cryostat section of the cerebellum of a GAD67-GFP mouse. A large number of neurons in the molecular layer of the cerebellum express GFP. **b** Overview image of a cryostat section of the lungs of a GAD67-GFP mouse. Several groups of GFP-fluorescent cells can be seen in the airway epithelium (*green* GFP fluorescence; *arrows*). The *red* channel shows nonspecific background fluorescence. **c–e** Single immunostaining for CGRP (*red* Cy3 fluorescence) in a GAD67-GFP (*green* GFP fluorescence) mouse lung cryosection. **c** *Green* channel showing GAD67-GFP fluorescence in an intraepithelial cell group. **d** CGRP-ir NEB and contacting C-fiber like nerve terminals (*arrowheads*). **e** Combination of the *red* and *green* channel, revealing that the distinct GFP-expressing cell group in the airway epithelium can be identified as a pulmonary NEB. Note that the nerve terminals do not express GFP. **f–i** Double immunolabeling for GAD65/67 (*red* Cy3 fluorescence) and CGRP (artificial *blue* color for Cy5 emission in far red) in a GAD67-GFP (*green* GFP fluorescence) mouse lung cryosection. **f** Red channel showing a GAD65/67-ir cell group (*arrowheads*) in the epithelium of an intrapulmonary airway. **g** *Green* channel with a GAD67-GFP-expressing NEB. **h** Combination of the red and green channel revealing that GFP-expressing cells fully colocalize with GAD65/67-ir NEB cells. Note that GFP-fluorescence is also present in NEB cell nuclei. **i** Combination of the three channels showing the expression of GAD65/67 and CGRP in GFP-positive NEB cells. *L* lumen of an airway ▶

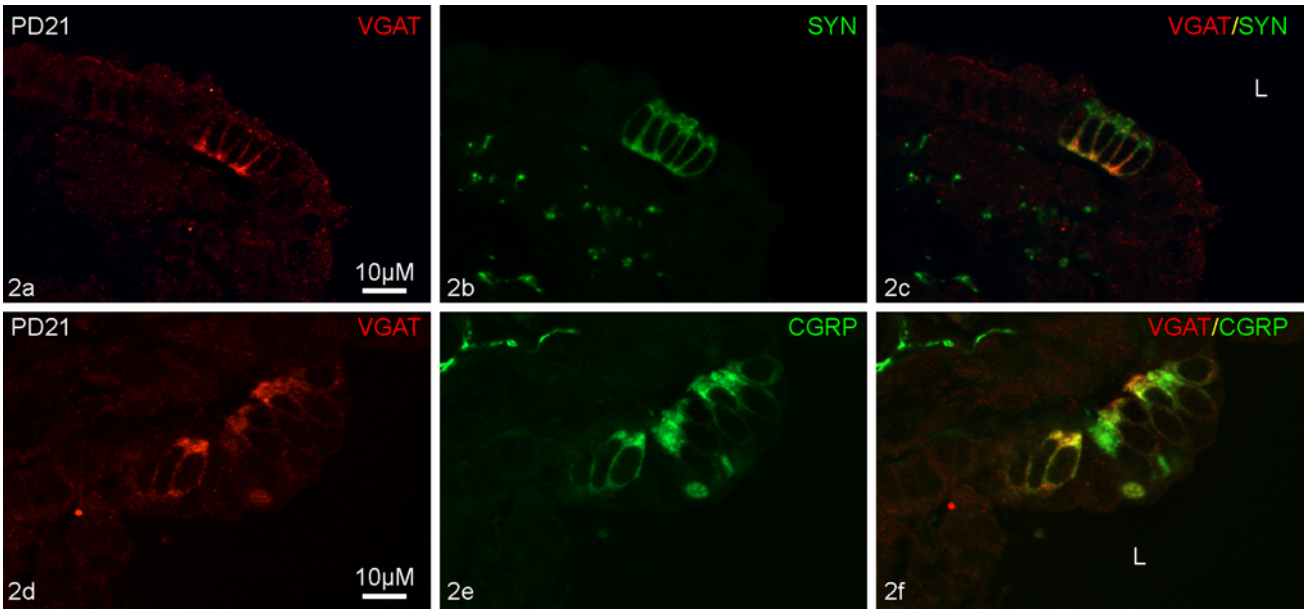

Fig. 2 **a–c** Double immunolabeling for the vesicular GABA transporter (VGAT; *red* Cy3 fluorescence) and synaptophysin (SYN; *green* FITC fluorescence), a marker for NEB cells. **a** VGAT-ir intraepithelial cell group. **b** Synaptophysin-ir NEB cells. **c** Combination of the two channels showing that VGAT is selectively expressed in NEB cells. **d–f** Double immunolabeling for VGAT (*red* Cy3 fluorescence) and CGRP (*green* Dylight488 fluorescence). **d** VGAT-ir intraepithelial cell group. **e** CGRP-ir NEB cells. **f** Combination of the two channels revealing a considerable colocalization between CGRP and VGAT. *L* lumen of an airway

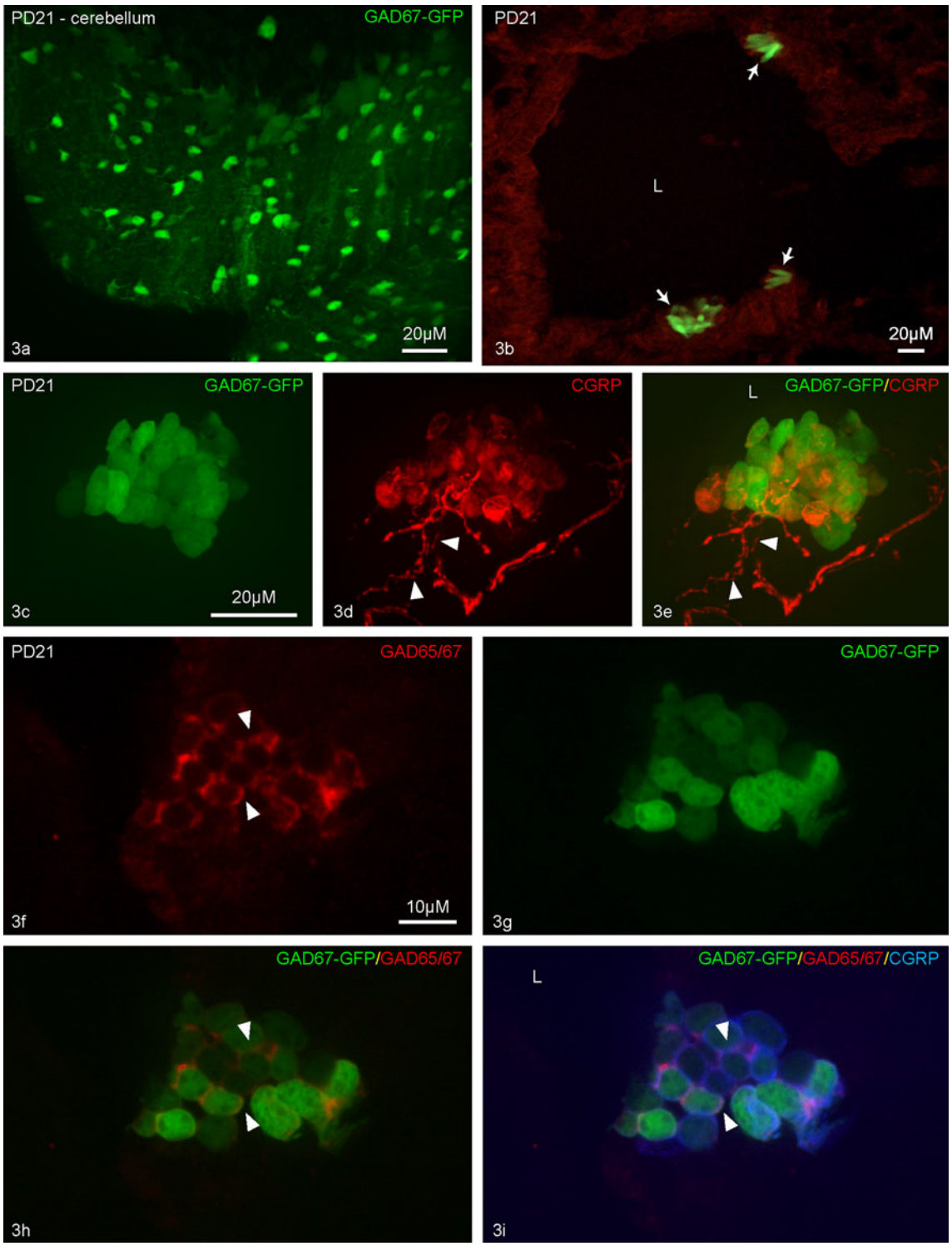

Results

GAD and VGAT expression in the wt C57-Bl6 mouse lung

Immunostaining for the GABA-synthesizing enzyme GAD65/67 revealed immunoreactivity (IR) in cell groups located in the airway epithelium in cryostat sections of prenatal (Fig. 1a), 3-week-old (Fig. 1d) and adult (Fig. 1g) mice. Double staining with calcitonin gene-related peptide (CGRP) as a selective marker for NEBs, identified all GAD65/67-expressing epithelial cell groups as NEBs (Fig. 1b, c, e, f, h, i). Typically, CGRP IR was more pronounced in the basal part of the cytoplasm, displaying a

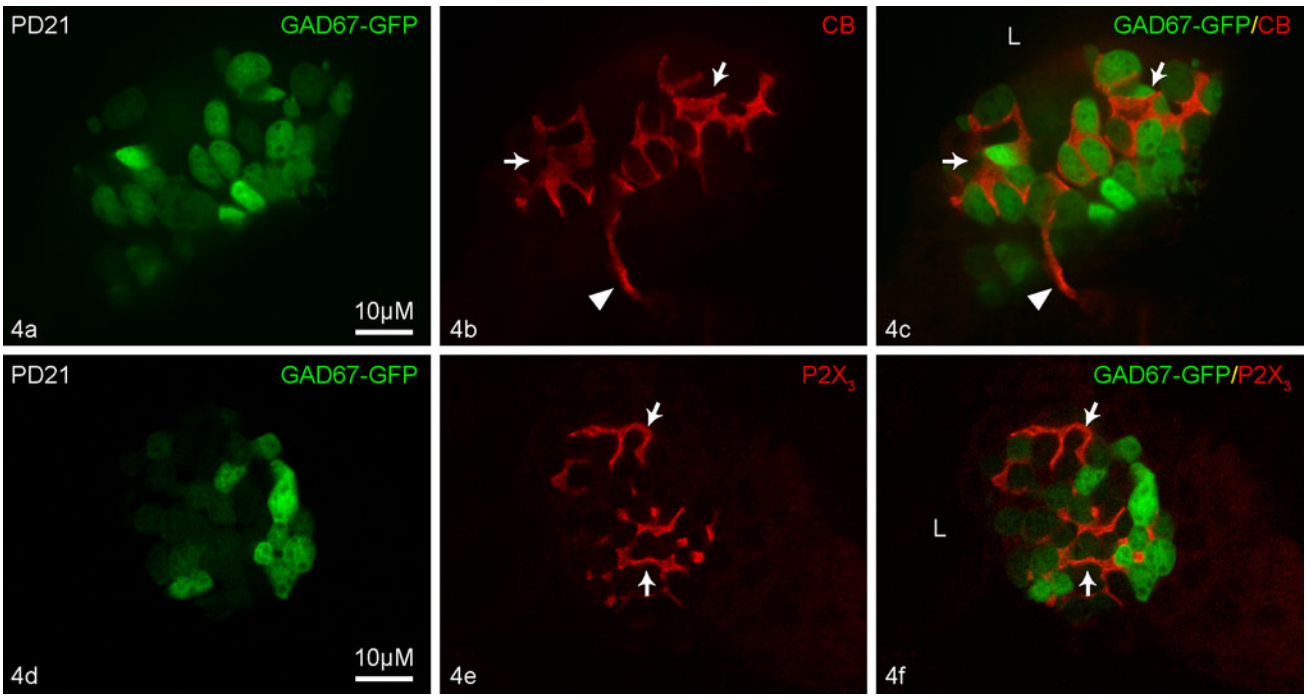

Fig. 4 **a–c** Immunostaining for CB (*red* Cy3 fluorescence) to mark the VGLUT/CB-ir vagal myelinated sensory component of the innervation of NEBs in a GAD67-GFP (*green* GFP fluorescence) mouse lung cryosection. **a** GAD67-GFP-expressing NEB. **b** The approaching CB-ir nerve fiber (*arrowhead*) branches and the terminals (*arrows*) penetrate between the epithelial cells. **c** Combination of the two channels revealing that the GFP-expressing NEB is innervated by a CB-positive nerve fiber, which provides extensive laminar terminals that surround the NEB cells. Also note the absence of GFP expression in the nerve terminals. **d–f** Immunostaining for $P2X_3$ (*red* Cy3 fluorescence), a marker for the $P2X_{2/3}$-ir population of the vagal myelinated sensory innervation of NEBs, in a GAD67-GFP (*green* GFP fluorescence) mouse lung cryosection. **d** GAD67-GFP-expressing NEB. **e** Intraepithelial arborization of $P2X_3$-ir nerve terminals (*arrows*). **f** Combination of the two channels revealing that the GFP-expressing NEB is innervated by a GFP-negative $P2X_3$-ir nerve fiber that branches between the NEB cells. *L* lumen of an airway

granular staining pattern, while GAD65/67 labeling apparently resulted in a more uniform staining of the NEB cell cytoplasm.

Multiple immunocytochemical staining for GAD65/67, CGRP and calbindin D-28 k (CB), as a marker of the vagal sensory innervation of mouse pulmonary NEBs (Brouns et al. 2009), revealed that NEB-related vagal sensory nerve terminals do not express GAD65/67 (Fig. 1j–m). Labeling with Clara cell specific protein (CCSP), a marker for Clara and Clara-like cells, revealed no expression of GAD65/67 in Clara-like cells (Fig. 1n–q), confirming that in the NEB microenvironment in mouse airways GAD65/67 is exclusively expressed in NEB cells.

Immunofluorescent labeling of the vesicular GABA transporter (VGAT) revealed IR in cell groups in the airway epithelium in cryostat sections of 3-week-old mice (Fig. 2a). Double staining with synaptophysin (Fig. 2b), reported as a marker for PNECs (Lee et al. 1987), identified all VGAT-expressing epithelial cells as NEB cells (Fig. 2c). Labeling for VGAT and CGRP (Fig. 2d, e) showed that the VGAT IR was granular and more pronounced in the basal part of the cytoplasm, similar to the CGRP IR (Fig. 2f).

Characterization of GFP-expressing cell groups in the airways of GAD67-GFP mice

Studying the GFP expression in brain cryosections of GAD67-GFP mice as a positive control, revealed a large number of GFP-positive neurons cells in the cerebellar cortex (Fig. 3a). In cryosections of the lungs of prenatal (ED18), 3-week-old (Fig. 3b) and adult GAD67-GFP mice, GFP-expressing cell groups were observed in the airway epithelium. Immunostaining for CGRP showed that all GFP-fluorescent cell groups were CGRP-immunoreactive (ir), and vice versa (Fig. 3c–e), invariably identifying the GFP-fluorescent intraepithelial cell groups as NEBs. Immunofluorescent labeling for GAD65/67 in GAD67-GFP mouse lungs demonstrated expression of this enzyme exclusively in all GFP-fluorescent NEB cells (Fig. 3f–i). Not all of the NEB cells seemed to express GFP-fluorescence with the same intensity, and GFP-fluorescence appeared to be spread

over the cytoplasm and nucleus. As in wt C57-Bl6 mice, GAD65/67 IR was also spread over the entire cytoplasm of NEB cells in GAD67-GFP mice (Fig. 3i).

Vagal sensory innervation of NEBs in GAD67-GFP mice

Immunostaining for CB, as a marker for the vesicular glutamate transporter (VGLUT)/CB-ir vagal sensory component of the innervation of mouse NEBs (Brouns et al. 2009), showed that part of the GFP-expressing NEBs are contacted by CB-positive nerve fibers in GAD67-GFP mouse airways (Fig. 4a–c). The approaching CB-ir nerve fibers branch, penetrate between the epithelial cells, and provide characteristic extensive laminar terminals that surround the NEB cells. Immunostaining for the ATP receptor $P2X_3$, a marker for the $P2X_{2/3}$-ir population of the vagal sensory innervation of NEBs (Brouns et al. 2009),

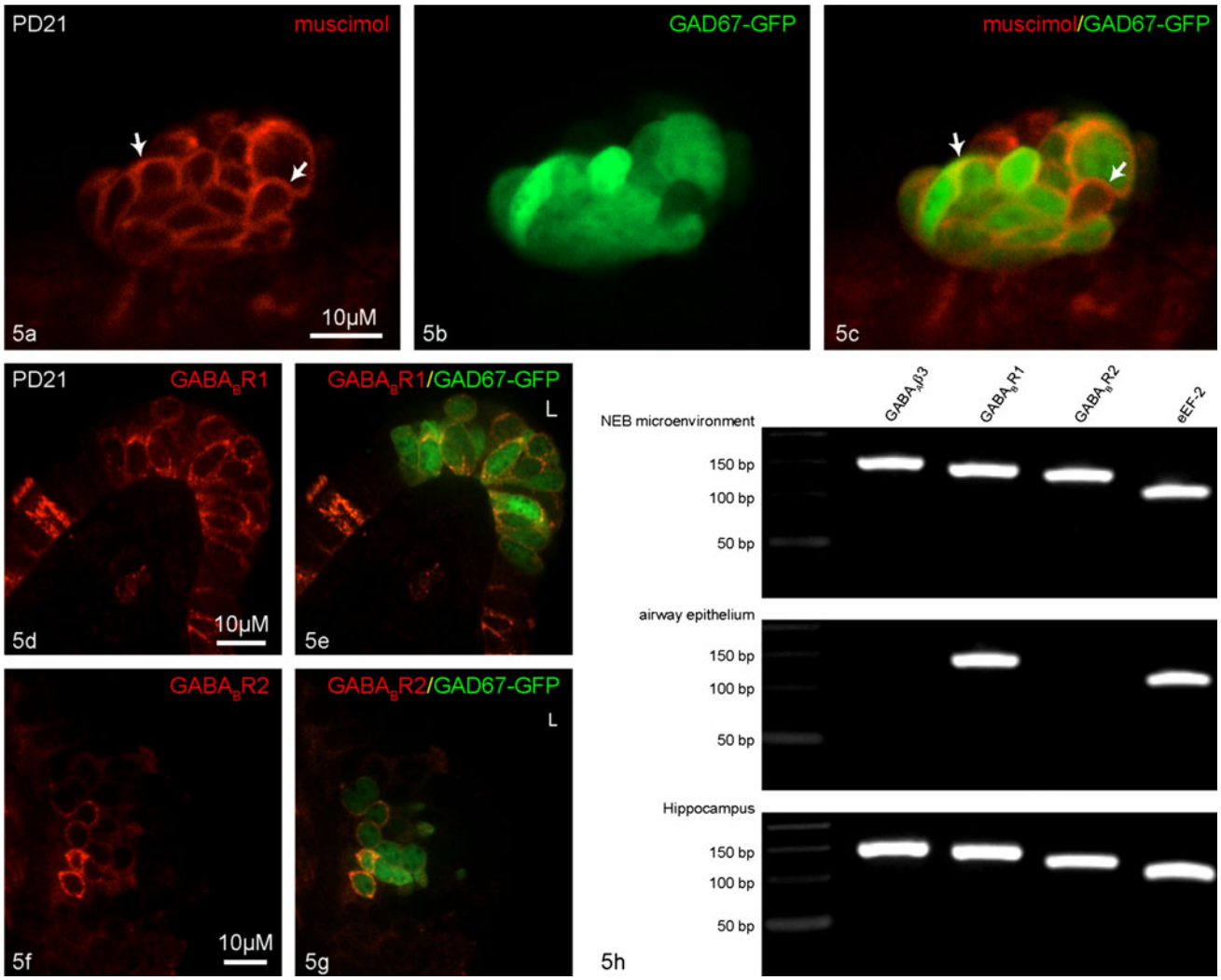

Fig. 5 **a–c** Binding of BODIPY TMR-X muscimol (*red* TMR fluorescence), a selective $GABA_A$ receptor ligand, in a live GAD67-GFP (*green* GFP fluorescence) mouse lung slice. **a** *Red* channel revealing a membrane localization of muscimol-labeled $GABA_A$ receptors on an airway epithelial cell group (*arrows*). **b** *Green* channel showing a GFP-expressing NEB. **c** Combined red and green channel facilitate identification of the $GABA_A$ receptor-expressing cells as NEB cells. **d**, **e** Immunostaining for $GABA_B$ receptor 1 ($GABA_BR1$; *red* Cy3 fluorescence) in a cryosection of GAD67-GFP (*green* GFP fluorescence) mouse lungs. **d** *Red* channel showing $GABA_BR1$ labeling in airway epithelial cells. **e** Combination of the red and green channel reveals that GFP-fluorescent NEB cells and ciliated cells express $GABA_BR1$. **f**, **g** Immunostaining for $GABA_BR2$ (*red* Cy3 fluorescence) in a GAD67-GFP (*green* GFP fluorescence) mouse lung cryosection. **f** Red channel showing $GABA_BR2$-positive epithelial cells. **g** Combination of the red and green channel allows identification of the $GABA_BR2$-ir cells as GFP-fluorescent NEB cells. *L* lumen of an airway. **h** RT-PCR for $GABA_A\beta3$ (*lane 1*), $GABA_BR1$ (*lane 2*) and $GABA_BR2$ (*lane 3*), and the housekeeping gene eEF-2 (*lane 4*) in laser microdissection samples of NEB microenvironment, control intrapulmonary airway epithelium, and hippocampus (positive control) of a GAD67-GFP mouse (PD14). *Left lane* DNA ladder (*bp* base pairs). $GABA_A\beta3$ and $GABA_BR2$ were detected in the NEB microenvironment, but its expression could not be demonstrated in control airway epithelium. $GABA_BR1$ mRNA could be detected both in the NEB microenvironment and in airway epithelium. eEF-2 was strongly expressed in all samples

showed that part of the GFP-expressing NEBs are contacted by $P2X_3$-positive nerve terminals that branch between the NEB cells (Fig. 4d–f). Both subpopulations of the vagal sensory innervation of NEBs lacked GAD67-GFP fluorescence.

Expression of GABA receptors in the NEB microenvironment

Real-time binding of BODIPY TMR-X muscimol on its molecular receptor, $GABA_A$, in live GAD67-GFP mouse lung slices, revealed a clear localization of $GABA_A$ receptors on the plasma membrane of NEB cells (Fig. 5a–c).

In cryosections of GAD67-GFP mouse lungs $GABA_BR1$ and $GABA_BR2$ immunostaining appeared to be co-expressed in NEB cells, as judged from the full colocalization with GFP-fluorescence. $GABA_BR1$ IR (but not $GABA_BR2$) was additionally seen in ciliated cells (Fig. 5d–g).

RT-PCR, carried out on samples of GAD67-GFP-positive NEBs and control airway epithelium that were laser microdissected from mouse lung cyrosections, showed a clear presence of GABA receptors. The expression of mRNA encoding $GABA_A\beta3$ and $GABA_BR2$ could be selectively demonstrated in the NEB microenvironment, while $GABA_BR1$ mRNA was detected in both the NEB microenvironment and control airway epithelium samples (Fig. 5h).

The mouse hippocampus, used as a positive control, showed expression of mRNA encoding all three receptors (Fig. 5h). The housekeeping gene, eEF-2, could be well detected in all samples (Fig. 5h), while the no-template controls for all receptors and for eEF-2 showed no amplification (data not shown).

Functional LCI of the NEB microenvironment in ex vivo lung slices of GAD67-GFP mice

Identification of NEBs in ex vivo lung slices of GAD67-GFP mice

Unfixed ex vivo lung slices of GAD67-GFP mice were stained with the red-fluorescent styryl pyridinium dye 4-Di-2-ASP (Pintelon et al. 2005). Correlation of 4-Di-2-ASP labeled NEBs and GFP-fluorescent cell groups in live lung slices revealed that the GFP-fluorescent intraepithelial groups (Fig. 6a), invariably correspond to 4-Di-2-ASP labeled NEBs (Fig. 6b).

Changes in 4-Di-2-ASP fluorescence intensity can also serve as an indicator for the mitochondrial membrane potential (De Proost et al. 2008). As a proof of concept, 4-Di-2-ASP loaded mouse lung slices of GAD67-GFP lungs were challenged with carbonylcyanide-4-(trifluoromethoxy) phenylhydrazone (FCCP; 10 μM; 10 s), a H^+ ionophore that uncouples oxidative phosphorylation and depolarizes mitochondria. Application of FCCP evoked a simultaneous increase in 4-Di-2-ASP fluorescence in all NEB cells and in ciliated epithelial cells (Fig. 6c–e). No alterations in 4-Di-2-ASP fluorescence were observed in the virtually non-stained Clara and Clara-like cells.

Measuring changes in the intracellular calcium concentration in GAD67-GFP mouse airways

Microscopic visualization of the epithelium from the luminal surface of longitudinally sectioned airways loaded with the red calcium indicator FluoForte revealed a baseline fluorescence pattern that was very similar to loading with Fluo-4 (De Proost et al. 2008): a widespread population of polygonal epithelial cells that emitted a much brighter fluorescence than the remainder of the more rounded epithelial cells (Fig. 7b). The fluorescent cell population typically corresponds to ciliated cells, and the virtually non-fluorescent cell population to Clara cells.

Short-term stimulation of FluoForte-loaded lung slices with 10 μM ATP (10 s) caused a reversible and reproducible cytoplasmic rise in FluoForte fluorescence, indicative of a rise in $[Ca^{2+}]_i$ in all Clara cells and to a lesser extent also in ciliated cells (Fig. 7a–c). ATP stimulation also caused a $[Ca^{2+}]_i$ rise in Clara-like cells, but never in NEB cells (results not shown). Stimulation of GAD67-GFP mouse lung slices with the established positive control stimulus for NEBs [50 mM $[K^+]_o$; 5 s; (De Proost et al. 2008)], resulted in a $[Ca^{2+}]_i$ rise in all NEB cells, and the typical delayed activation of surrounding Clara-like cells (Fig. 7d–h).

Discussion

The present study revealed that pulmonary NEBs comprise a selective expression site for GAD and VGAT in mouse lungs, and that $GABA_A$ and $GABA_B$ receptors are expressed in the NEB microenvironment. Apart from the interesting observation that a functional GABAergic signaling system is present in mouse NEBs, the selective expression of GAD65/67 in NEB cells allowed application of a GAD67-GFP mouse model for morphological, neurochemical, molecular and functional studies of the NEB microenvironment.

Immunostaining with an antibody that is able to detect both GAD65 and GAD67 isoforms, unraveled that only specific intraepithelial cell groups in the airways expressed GAD65/67. Double immunostaining with PNEC markers revealed that the stained cell groups invariably concerned

pulmonary NEBs. This observation is in line with an earlier description of GAD65/67 IR in mouse PNECs (Yabumoto et al. 2008), but is in contrast with a report of GAD IR in nearly all mouse airway epithelial cells (Xiang et al. 2007). The antibody used in the present study also appeared to detect GAD in monkey pulmonary NEBs (Fu and Spindel 2009). The precise location of GAD65/67 in the NEB microenvironment was unraveled by colabeling with CB and $P2X_3$, revealing that both populations of vagal myelinated afferents with extensive terminals between the NEB cells (Brouns et al. 2012) lacked GAD65/67 IR, as was also the case for CLCs. Together with the selective GFP-fluorescence in NEB cells in the GAD67-GFP mice, these observations allowed us to conclude that in mouse lungs, GAD is expressed in PNECs only.

In both wt C57-Bl6 and GAD67-GFP mice, double immunostaining for CGRP, reported to be present in mainly basally located secretory granules in mouse NEB

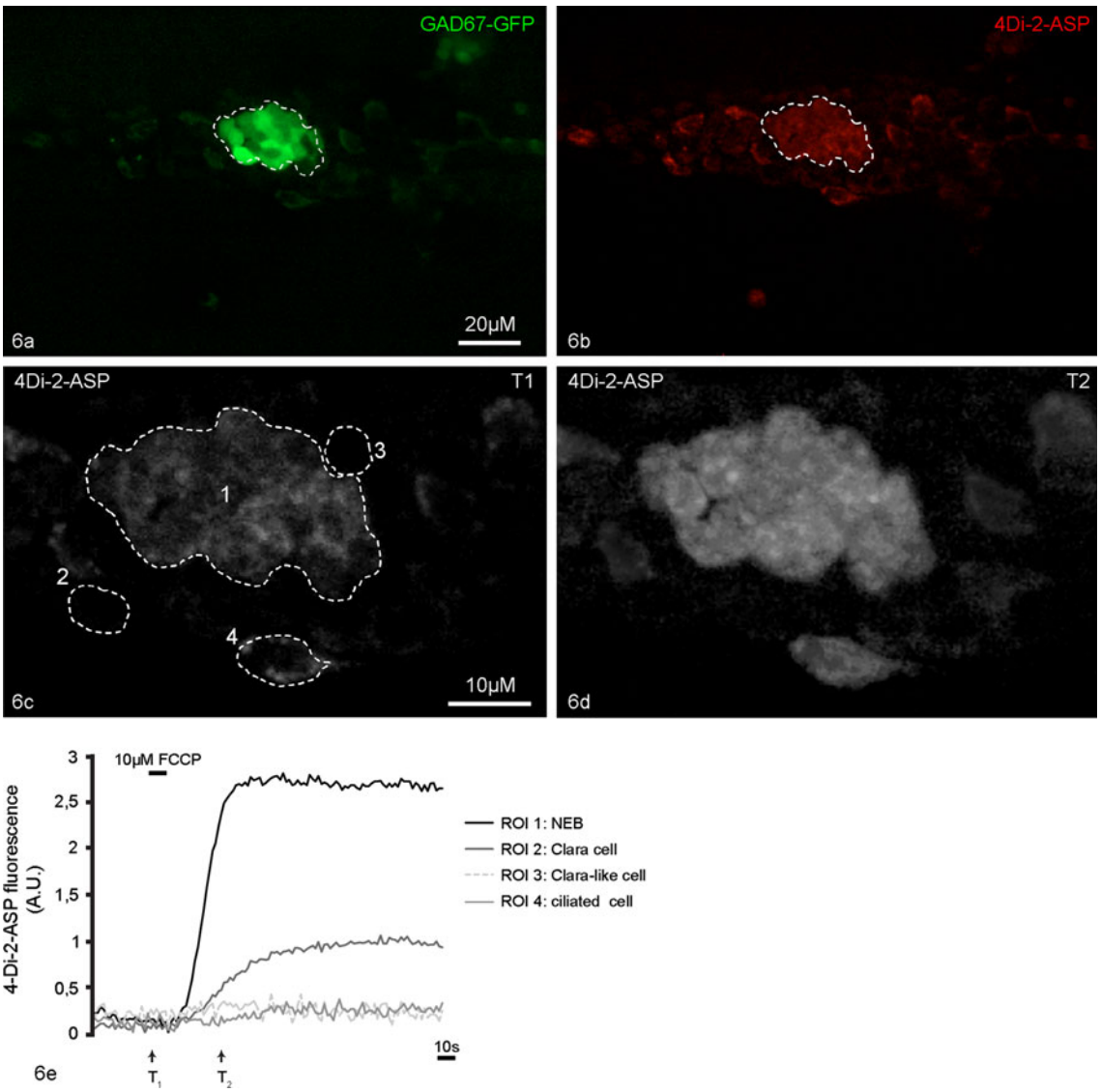

Fig. 6 Representative recording of mitochondrial membrane depolarization in GFP-fluorescent NEB cells and surrounding epithelial cells in an ex vivo lung slice of a GAD67-GFP mouse, before, during and after a 10 s challenge with 10 µM FCCP, which uncouples oxidative phosphorylation and depolarizes mitochondria. **a** *Green* channel showing a GAD67-GFP-expressing NEB. **b** *Red* channel shows that the lung slice was additionally loaded with the fluorescent styryl pyridinium dye 4-Di-2-ASP, which is both a mitochondrial membrane potential dye and a rather selective marker for live NEBs, and allows identification of the GFP-fluorescent cell groups as 4-Di-2-ASP-labeled NEBs (*encircled*). **c–d** Magnifications of **b** showing time-lapse images of 4-Di-2-ASP fluorescence intensity in the NEB and surrounding epithelial cells at different time points, indicated in the graph (**e**) as *T1* and *T2*. The marked regions of interest (ROIs) 1–4, respectively represent a NEB, a Clara cell, a CLC and a ciliated cell. **e** Graph plotting the time course of changes in 4-Di-2-ASP fluorescence intensity in arbitrary units (AU), as observed during administration of FCCP, which appears to evoke a simultaneous increase in 4-Di-2-ASP fluorescence in NEB cells and ciliated epithelial cells, although with a much lower intensity in the latter

cells (Brouns et al. 2009), did not result in a clear colocalization with GAD, which seemed to be evenly distributed over the entire NEB cell cytoplasm. However, the additional VGAT IR seen in NEB cells, with a predominantly basally located granular appearance, strongly suggests storage of GABA in a population of secretory vesicles.

Because of the considerable research interest in GABAergic neurons in the CNS, several GFP mouse models have been developed (Oliva et al. 2000; Zhao et al. 2010). In the commercially available model used in the present study, transgenic mice expressed EGFP under the control of GAD67 regulatory elements and have a single-copy gene for GAD67 expression, avoiding overexpression, and a single-copy gene for GFP expression (Zhao et al. 2010). This GAD67-GFP mouse strain does not encode an EGFP fusion protein, allowing for GFP to diffuse freely in the cytoplasm and fill the whole GFP-expressing cell (Tamamaki et al. 2003). Although both GFP and GAD67 are soluble proteins, their subcellular localization will probably differ, as described for GFP-positive cells in mouse brains. This explains our observation that GFP-fluorescence seemed to be spread over the entire cytoplasm and nucleus of labeled NEB cells. Cryostat sections of the cerebellum of the GAD67-GFP mouse strain, as a positive control, confirmed the strong GFP expression in GABAergic neurons that was reported for the same mouse model (Zhao et al. 2010).

The present study revealed a full overlap between GAD65/67-ir and GFP-expressing cells located in the airway epithelium in GAD67-GFP mice, further established that all GFP-fluorescent cell groups seen in lungs concerned pulmonary NEBs, and that all NEB cells expressed GFP. Similar GFP-positive PNEC-like cell groups have been reported in another GAD67-GFP mouse strain (Yabumoto et al. 2008). Since NEBs are known to differentiate very early in embryonic development, our observation of GFP expression in fetal GAD67-mice is an important step forward for functional NEB studies in fetal lung. Moreover, the finding of GFP expression in NEBs at ED18 and all postnatal ages indicates that GAD67 is expressed in NEBs throughout life and suggests multiple potential roles for GABA. Although brain studies report that different GAD67-GFP mouse models label different subpopulations of GABAergic neurons (Tamamaki et al. 2003; Zhao et al. 2010; Oliva et al. 2000), it is clear that in the adopted GAD67-GFP model all pulmonary NEB cells expressed GFP, although the fluorescence intensity often showed a considerable variation between the PNECs in individual NEBs. It has been proposed that differences in the level of GFP-fluorescence between cells in the same cell type could depend on the amount of GFP accumulated in the cells and does not necessarily reflect differences in GAD67 protein expression (Tamamaki et al. 2003). The presently used GAD67-GFP mouse model clearly allows unequivocal identification of NEBs by their GFP-fluorescence in both fixed and live mouse airway epithelium.

Fig. 7 **a–c** Representative recordings of changes in fluorescence intensity as measured in murine airway epithelial cells of FluoForte-loaded lung slices, before, during and after stimulation with ATP (10 μM, 10 s). **a** Graph plotting the time course of changes in FluoForte fluorescence intensity. ROIs 1–3 correspond to the Clara cells and a ciliated cell encircled in image **b**. **b**, **c** Images of FluoForte fluorescence in the airway epithelium at two different time points, indicated in the graph as *T1* and *T2*, which correspond to the images taken just before and after application of ATP. The Clara cells, and to a lesser extent also the ciliated cells, respond to ATP stimulation with a cytoplasmic rise in FluoForte fluorescence, corresponding to an increase in $[Ca^{2+}]_i$ that drops back to basal levels upon washout of ATP. **d–h** Representative recording of fluorescence changes measured in GFP-fluorescent NEB cells and surrounding CLCs, before, during and after a 5 s challenge with 50 mM $[K^+]_o$ in a FluoForte-loaded lung slice of a GAD67-GFP mouse. **d** Graph plotting the time course of changes in FluoForte fluorescence intensity. The ROIs in the graph correspond to the NEB (ROI 1) and 2 CLCs (ROI 2–3) as outlined in image **e**. **e** Green channel showing an image of the GFP-expressing NEB taken prior to the experiment. **f–h** Red channel showing time-lapse images of FluoForte fluorescence in the NEB microenvironment at different time points, indicated in the graph as *T0–T2*. NEB cells respond to a pulse of high $[K^+]_o$ with a fast rise in FluoForte fluorescence (*g*), representing a $[Ca^{2+}]_i$ rise, a few seconds earlier than the surrounding CLCs (*h*)

Thorough morphological and neurochemical examination of GFP-fluorescent NEBs in cryostat sections of GAD67-GFP mice, revealed characteristics indistinguishable from wt C57-Bl6 mice, including two different vagal sensory nerve fiber populations with intraepithelial nerve terminals that could be visualized with either CB (VGLUT/CB population) or $P2X_3$ ATP receptor immunostaining ($P2X_{2/3}$ population) (Brouns et al. 2012), enabling the use of the GAD67-GFP mouse model for our future functional and molecular studies of NEBs.

Functional studies of mouse pulmonary NEBs can be carried out on vibratome slices of live lung tissue (De Proost et al. 2008; Fu et al. 1999; Pintelon et al. 2005). Efficient LCI of pulmonary NEBs, however, critically depends on their unequivocal identification in the airway epithelium, which could be obtained in rodents by vital staining with the styryl pyridinium dye 4-Di-2-ASP (Pintelon et al. 2005) or neutral red (Fu et al. 1999). Staining of live lung slices of GAD67-GFP mice with 4-Di-2-ASP in the present study made clear that all of the GFP-fluorescent NEBs could be co-stained with 4-Di-2-ASP, although mostly much less clear. Whereas currently the staining procedure with 4-Di-2-ASP takes about 3 h, the use of mice with GFP-fluorescent NEBs in functional experiments allows for the immediate use of the slices, thereby considerably shortening and optimizing the functional imaging procedure.

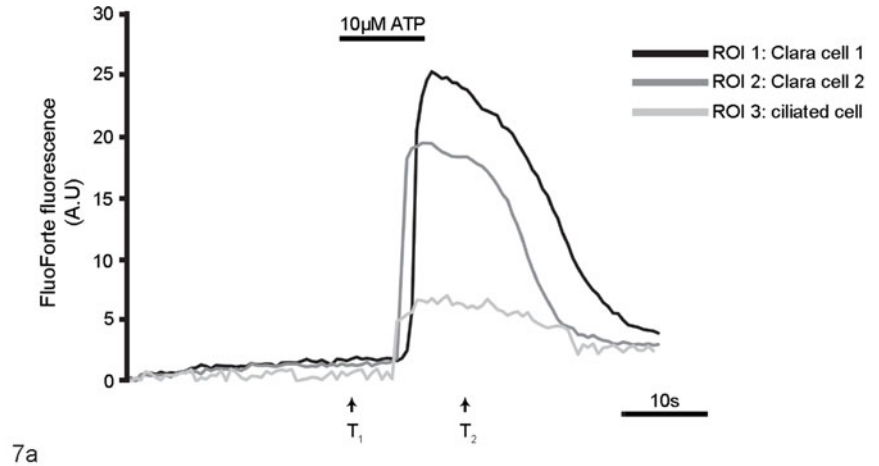

7a

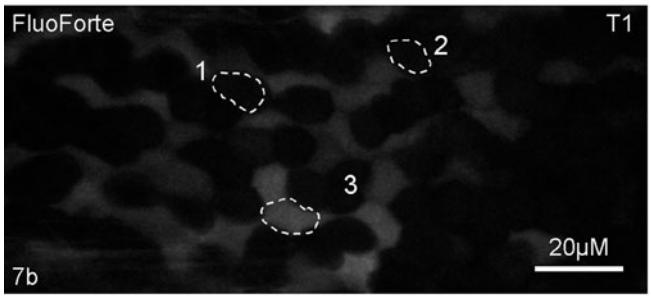

7b

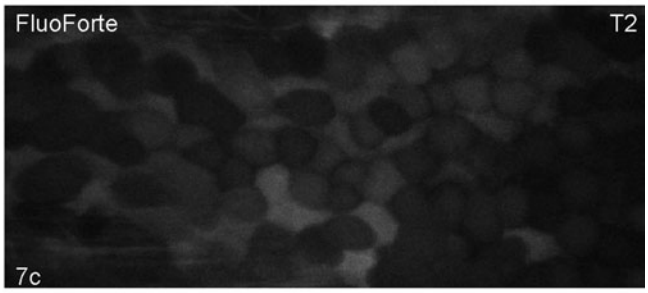

7c

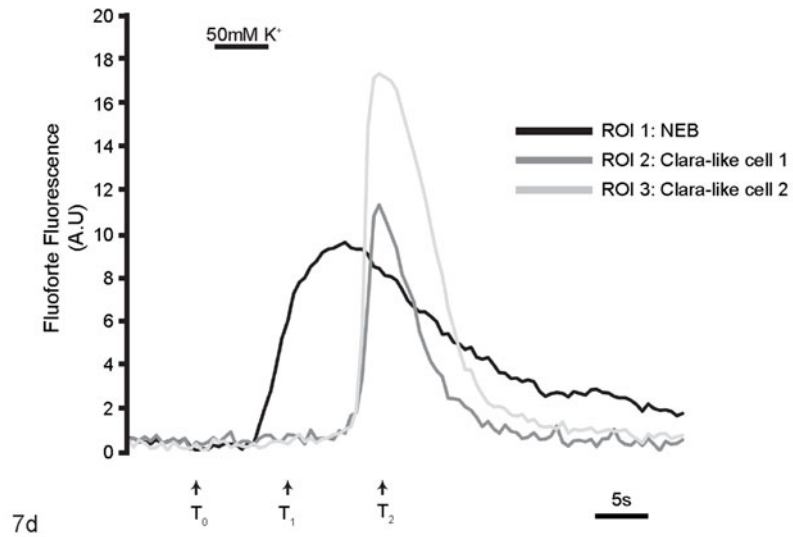

7d

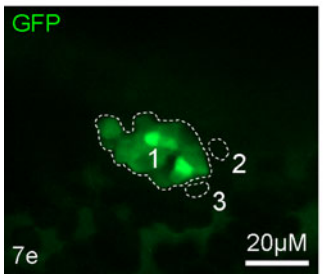

7e

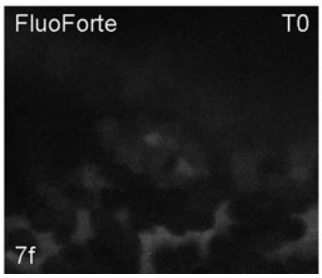

7f

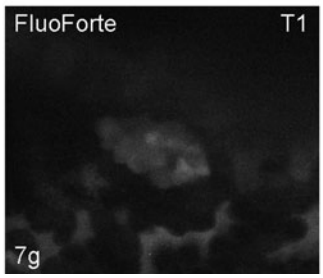

7g

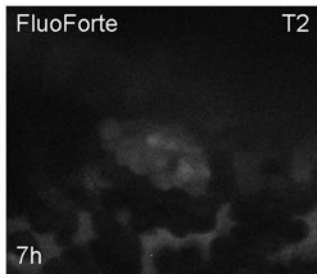

7h

In addition to the time-consuming but rather selective labeling of live rodent NEBs, the red-fluorescent signal of 4-Di-2-ASP, which accumulates in mitochondria, has been characterized as a sensitive probe for registering changes in the mitochondrial membrane potential (De Proost et al. 2008). In the present study, we used this property as a proof of principle for functional studies of NEBs in GAD67-GFP mice, whereby the responses of GFP-fluorescent NEB cells and ciliated cells to the mitochondrial uncoupler FCCP could easily be demonstrated, as reported for wt C57-Bl6 mice (De Proost et al. 2008).

Since activation of cells is often accompanied by changes in $[Ca^{2+}]_i$, establishing a fluorescent Ca^{2+} indicator protocol that is compatible for double labeling with the NEB marker is essential. In wt C57-Bl6 mice, with red 4-Di-2-ASP stained NEBs, we obtained good results with the green-fluorescent Fluo-4 for monitoring $[Ca^{2+}]_i$ (De Proost et al. 2008, 2009; Lembrechts et al. 2012). For the present GAD67-GFP model, with green GFP-fluorescent NEBs, the red-fluorescent calcium indicator FluoForte was optimized after a long search for suitable red-fluorescent Ca^{2+} indicators. FluoForte-loaded Clara cells and ciliated cells showed after application of 10 μM ATP a similar activation pattern as described earlier in airway epithelial cell models (Knowles et al. 1991), and in wt C57-Bl6 mouse lung slices using Fluo-4 (De Proost et al. 2008). To confirm proper loading of NEB cells with FluoForte in GAD67-mice, it was shown that a short control stimulus with high $[K^+]_o$ can be used, resulting in a reversible influx of extracellular Ca^{2+} as evidenced by a rise in FluoForte fluorescence. The latter is followed by the typical delayed activation of the Clara-like cells via release of ATP from activated NEBs, as described by (De Proost et al. 2009) using Fluo-4. The above proof of principle experiments established the good functionality of FluoForte as a red-fluorescent $[Ca^{2+}]_i$ indicator in GFP mouse models.

Since GAD65/67 IR and GFP expression under the GAD67 promotor allow the conclusion that cells are able to produce GABA and hence should be considered 'GABAergic' (Soghomonian and Martin 1998), the latter would also hold for NEB cells in fetal (ED18), postnatal and adult lungs. The functional significance of GABA synthesis in NEBs and its storage in secretory vesicles, as evidenced by the additional VGAT expression, remains to be determined. So far, little is known about the potential involvement of GABAergic signaling pathways in the lungs in health and disease.

GABA is an important signaling molecule, both inside and outside the CNS, and may serve a multitude of (patho)physiological functions. A relationship between GABAergic signaling and oncogenesis has been suggested based on the finding that the expression of different elements in the signaling cascade (GABA receptors, GAD) is altered in a variety of cancer cell types (Schuller et al. 2008; Young and Bordey 2009). Prenatal nicotine exposure was reported to recruit $GABA_A\beta3$ receptors in NEBs of the monkey lung (Fu and Spindel 2009). GABAergic signaling may therefore be involved in balancing cell proliferation and differentiation in the stem cell niche of the NEB microenvironment, in which recently PNECs were presented as the main cells of origin of small cell lung carcinomas (Sutherland et al. 2011).

$GABA_A$ and $GABA_B$ receptors have been reported in gastroesophageal vagal afferents (Page et al. 2006) and neuronal cell bodies of spinal afferent neurons (Paul et al. 2012). However, in the NEB microenvironment, the full colocalization of $GABA_BR1$ and R2 with GFP in GAD67-GFP mice—which is never seen after labeling of vagal afferents—indicates that no $GABA_B$ receptors are expressed on the vagal sensory terminals between NEB cells.

Our data on $GABA_B$ receptor expression are in contrast with Yabumoto et al. (2008) who described the observation of $GABA_B$ receptors in unidentified bronchial and alveolar epithelial cells, while we showed a selective $GABA_B$ receptor expression on mouse NEB cells. However, the data included in the present study are based on the use of different sets of antibodies for the two subunits of the $GABA_B$ receptor, revealing their coexpression on NEB cells. The latter strengthened our findings considering the fact that the $GABA_B$ receptor needs coexpression of both $GABA_BR1$ and $GABA_BR2$ to be functional.

Yabumoto et al. (2008) reported the detection of $GABA_A$ receptor mRNA in whole mouse lung tissue. This finding has now been confirmed by receptor binding of the selective fluorescent $GABA_A$ receptor agonist BODIPY TMR-X muscimol in live mouse lung slices, further revealing that $GABA_A$ receptors are expressed on NEB cells.

Additionally, we confirmed the location of both $GABA_A$ and $GABA_B$ (R1 and R2) receptor mRNA expression by the use of selective LMD of the NEB microenvironment and subsequent RT-PCR.

In conclusion, the present study not only revealed the presence of a GABAergic signaling pathway and unraveled the detailed location of the GABA-synthesizing enzyme GAD, the vesicular GABA transporter and GABA receptors in the NEB microenvironment, but also the very selective expression of GFP in pulmonary NEBs in a GAD67-GFP mouse model. This model allows straightforward morphological, neurochemical and gene expression analysis of GFP-fluorescent NEBs. Different proof of concept experiments have clearly shown that application of the GAD67-GFP mouse model represents a powerful tool for future functional NEB studies using our established ex vivo lung slice model for confocal molecular LCI of the mouse NEB microenvironment.

Acknowledgments This study was supported by grants of the Fund for Scientific Research-Flanders (FWO; G.0589.11 to D.A. and J-P.T.), the Hercules Foundation (AUAH-09-001 to D.A.) and the University of Antwerp (GOA BOF 2007 to D.A. and KP BOF 2011 to I.B.). We thank Prof. Dr. L.-Y. Lee (University of Kentucky, Lexington, KY, USA) for his initial help with introducing GAD67-GFP mice into our research, F. Terloo for technical assistance, D. De Rijck for help with imaging and illustrations, D. Vindevogel for aid with the manuscript, and S. Kockelberg for administrative help.

References

Adriaensen D, Brouns I, Van Genechten J, Timmermans J-P (2003) Functional morphology of pulmonary neuroepithelial bodies: extremely complex airway receptors. Anat Rec 270A:25–40

Adriaensen D, Brouns I, Pintelon I, De Proost I, Timmermans JP (2006) Evidence for a role of neuroepithelial bodies as complex airway sensors: comparison with smooth muscle-associated airway receptors. J Appl Physiol 101:960–970

Bormann J (2000) The 'ABC' of GABA receptors. Trends Pharmacol Sci 21:16–19

Borodinsky LN, Spitzer NC (2007) Activity-dependent neurotransmitter-receptor matching at the neuromuscular junction. Proc Natl Acad Sci USA 104:335–340

Brouns I, Oztay F, Pintelon I, De Proost I, Lembrechts R, Timmermans JP, Adriaensen D (2009) Neurochemical pattern of the complex innervation of neuroepithelial bodies in mouse lungs. Histochem Cell Biol 131:55–74

Brouns I, Pintelon I, Timmermans JP, Adriaensen D (2012) Novel insights in the neurochemistry and function of pulmonary sensory receptors. Adv Anat Embryol Cell Biol 211:1–115

Bu DF, Erlander MG, Hitz BC, Tillakaratne NJ, Kaufman DL, Wagner-McPherson CB, Evans GA, Tobin AJ (1992) Two human glutamate decarboxylases, 65-kDa GAD and 67-kDa GAD, are each encoded by a single gene. Proc Natl Acad Sci USA 89:2115–2119

Cutz E, Jackson A (1999) Neuroepithelial bodies as airway oxygen sensors. Respir Physiol 115:201–214

Cutz E, Fu XW, Yeger H, Peers C, Kemp PJ (2003) Oxygen sensing in pulmonary neuroepithelial bodies and related tumor cell models. In: Lahiri S, Semenza GL, Prabhakar NR (eds) Lung oxygen sensing. Marcel Dekker, New York, pp 567–602

De Proost I, Pintelon I, Brouns I, Kroese ABA, Riccardi D, Kemp PJ, Timmermans JP, Adriaensen D (2008) Functional live cell imaging of the pulmonary neuroepithelial body microenvironment. Am J Respir Cell Mol Biol 39:180–189

De Proost I, Pintelon I, Wilkinson WJ, Goethals S, Brouns I, Van Nassauw L, Riccardi D, Timmermans JP, Kemp PJ, Adriaensen D (2009) Purinergic signaling in the pulmonary neuroepithelial body microenvironment unraveled by live cell imaging. FASEB J 23:1153–1160

Fu XW, Spindel ER (2009) Recruitment of GABA(A) receptors in chemoreceptor pulmonary neuroepithelial bodies by prenatal nicotine exposure in monkey lung. Adv Exp Med Biol 648:439–445

Fu XW, Nurse CA, Wang YT, Cutz E (1999) Selective modulation of membrane currents by hypoxia in intact airway chemoreceptors from neonatal rabbit. J Physiol 514:139–150

Fu XW, Wang D, Nurse CA, Dinauer MC, Cutz E (2000) NADPH oxidase is an O_2 sensor in airway chemoreceptors: evidence from K^+ current modulation in wild-type and oxidase-deficient mice. Proc Natl Acad Sci USA 97:4374–4379

Kaufman DL, Houser CR, Tobin AJ (1991) Two forms of the gamma-aminobutyric acid synthetic enzyme glutamate decarboxylase have distinct intraneuronal distributions and cofactor interactions. J Neurochem 56:720–723

Kemp PJ, Searle GJ, Hartness ME, Lewis A, Miller P, Williams S, Wootton P, Adriaensen D, Peers C (2003) Acute oxygen sensing in cellular models: relevance to the physiology of pulmonary neuroepithelial and carotid bodies. Anat Rec 270:41–50

Knowles MR, Clarke LL, Boucher RC (1991) Activation by extracellular nucleotides of chloride secretion in the airway epithelia of patients with cystic fibrosis. N Engl J Med 325:533–538

Kouadjo KE, Nishida Y, Cadrin-Girard JF, Yoshioka M, St-Amand J (2007) Housekeeping and tissue-specific genes in mouse tissues. BMC Genomics 8:127

Lauweryns JM, Van Lommel A (1986) Effect of various vagotomy procedures on the reaction to hypoxia of rabbit neuroepithelial bodies: modulation by intrapulmonary axon reflexes. Exp Lung Res 11:319–339

Lauweryns JM, Cokelaere M, Theunynck P (1972) Neuroepithelial bodies in the respiratory mucosa of various mammals. A light optical, histochemical and ultrastructural investigation. Z Zellforsch Mikrosk Anat 135:569–592

Lee I, Gould VE, Moll R, Wiedenmann B, Franke WW (1987) Synatophysin expressed in the bronchopulmonary tract: neuroendocrine cells, neuroepithelial bodies, and neuroendocrine neoplasms. Differentiation 34:115–125

Lembrechts R, Pintelon I, Schnorbusch K, Timmermans JP, Adriaensen D, Brouns I (2011) Expression of mechanogated Two-pore-domain potassium channels in mouse lungs: special reference to mechanosensory airway receptors. Histochem Cell Biol 136:371–385

Lembrechts R, Brouns I, Schnorbusch K, Pintelon I, Timmermans JP, Adriaensen D (2012) Neuroepithelial bodies as mechanotransducers in the intrapulmonary airway epithelium: involvement of TRPC5. Am J Respir Cell Mol 47(3):315–323

Linnoila RI (2006) Functional facets of the pulmonary neuroendocrine system. Lab Invest 86:425–444

Majchrzak M, Di SG (2000) GABA and muscimol as reversible inactivation tools in learning and memory. Neural Plast 7:19–29

McIntire SL, Reimer RJ, Schuske K, Edwards RH, Jorgensen EM (1997) Identification and characterization of the vesicular GABA transporter. Nature 389:870–876

Oliva AA Jr, Jiang M, Lam T, Smith KL, Swann JW (2000) Novel hippocampal interneuronal subtypes identified using transgenic mice that express green fluorescent protein in GABAergic interneurons. J Neurosci 20:3354–3368

Page AJ, O'Donnell TA, Blackshaw LA (2006) Inhibition of mechanosensitivity in visceral primary afferents by GABAB receptors involves calcium and potassium channels. Neuroscience 137:627–636

Pan J, Copland I, Post M, Yeger H, Cutz E (2006) Mechanical stretch-induced serotonin release from pulmonary neuroendocrine cells: implications for lung development. Am J Physiol Lung Cell Mol Physiol 290:L185–L193

Paul J, Zeilhofer HU, Fritschy JM (2012) Selective distribution of GABA(A) receptor subtypes in mouse spinal dorsal horn neurons and primary afferents. J Comp Neurol 520:3895–3911

Pintelon I, De Proost I, Brouns I, Van Herck H, Van Genechten J, Van Meir F, Timmermans JP, Adriaensen D (2005) Selective visualisation of neuroepithelial bodies in vibratome slices of living lung by 4-Di-2-ASP in various animal species. Cell Tissue Res 321:21–33

Saito K, Kakizaki T, Hayashi R, Nishimaru H, Furukawa T, Nakazato Y, Takamori S, Ebihara S, Uematsu M, Mishina M, Miyazaki J, Yokoyama M, Konishi S, Inoue K, Fukuda A, Fukumoto M, Nakamura K, Obata K, Yanagawa Y (2010) The physiological roles of vesicular GABA transporter during embryonic development: a study using knockout mice. Mol Brain 3:40

Scheuermann DW (1987) Morphology and cytochemistry of the endocrine epithelial system in the lung. Int Rev Cytol 106:35–88

Schuller HM, Al-Wadei HA, Majidi M (2008) Gamma-aminobutyric acid, a potential tumor suppressor for small airway-derived lung adenocarcinoma. Carcinogenesis 29:1979–1985

Soghomonian JJ, Martin DL (1998) Two isoforms of glutamate decarboxylase: why? Trends Pharmacol Sci 19:500–505

Sorokin SP, Hoyt RFJ (1989) Neuroepithelial bodies and solitary small-granule cells. In: Massaro D (ed) Lung cell Biology. Marcel Dekker, New York, pp 191–344

Sorokin SP, Hoyt RFJ (1990) On the supposed function of neuroepithelial bodies in adult mammalian lungs. News Physiol Sci 5:89–95

Sutherland KD, Proost N, Brouns I, Adriaensen D, Song J-Y, Berns A (2011) Cells of origins of small cell lung cancer: inactivation of Trp53 and Rb1 in distinct cell types of adult mouse lung. Cancer Cell 19:754–764

Tamamaki N, Yanagawa Y, Tomioka R, Miyazaki J, Obata K, Kaneko T (2003) Green fluorescent protein expression and colocalization with calretinin, parvalbumin, and somatostatin in the GAD67-GFP knock-in mouse. J Comp Neurol 467:60–79

Xiang YY, Wang S, Liu M, Hirota JA, Li J, Ju W, Fan Y, Kelly MM, Ye B, Orser B, O'Byrne PM, Inman MD, Yang X, Lu WY (2007) A GABAergic system in airway epithelium is essential for mucus overproduction in asthma. Nat Med 13:862–867

Yabumoto Y, Watanabe M, Ito Y, Maemura K, Otsuki Y, Nakamura Y, Yanagawa Y, Obata K, Watanabe K (2008) Expression of GABAergic system in pulmonary neuroendocrine cells and airway epithelial cells in GAD67-GFP knock-in mice. Med Mol Morphol 41:20–27

Young SZ, Bordey A (2009) GABA's control of stem and cancer cell proliferation in adult neural and peripheral niches. Physiology (Bethesda) 24:171–185

Zhao S, Zhou Y, Gross J, Miao P, Qiu L, Wang D, Chen Q, Feng G (2010) Fluorescent labeling of newborn dentate granule cells in GAD67-GFP transgenic mice: a genetic tool for the study of adult neurogenesis. PLoS One 5:e12506